Genesis Determination of Single Crystal Quartz Varieties (α-SiO_2): Distinguishing Natural Amethyst from Synthetic

By M.P.H. Curti [1]; T. Rozet [2]; V. Fejoz [2] W. Oei [2] and G. Musilli [3]

[1] Bellerophon Gemlab PVT, Ltd , 8/808 One Galle Face, 00200 Colombo, Sri Lanka
[2] Bellerophon Gemlab Co,Ltd, 26-28 Mahesak soi 3, 10500 Bangkok, Thailand
[3] Bellerophon Gemlab SAS, 16 Place Vendôme, 75001 Paris, France

Introduction

Synthetic quartz has been grown in laboratories for over a century, with the earliest documented success in 1851 by H. de Senarmont (Nassau, 1980). Today, the synthetic quartz industry is well-established, driven by its extensive industrial applications (Byrappa and Yoshimura, 2001).

The process of growing man-made quartz closely mirrors the hydrothermal conditions under which most natural quartz forms (Laudise, 1959). This similarity poses significant challenges for gemological laboratories in accurately determining the genesis of quartz varieties, particularly for the most expensive variety amethyst.

For decades, the gemstone industry has contended with a substantial presence of synthetic quartz, prompting extensive research into reliable identification techniques for synthetic amethyst (Crowningshield et al., 1986; Fritsch and Rossman, 1987, Karempelas et al., 2011; Balitsky et al., 2004).

However, these methods may remain inconclusive when used individually and often fail to address their inherent limitations. In this study, we explore established techniques, investigate their potential underlying causes, and integrate our new findings to enhance differentiation between natural and synthetic quartz.

Material & Methods

A total of 1300 samples ranging from 0.76 to 6.78 carats were selected for this study (Table 1), comprising 50 samples of each genesis (natural and synthetic) for colorless quartz, citrine, and smoky quartz. This study places a major emphasis on amethysts, with 500 natural and 500 synthetic samples, due to their prevalence as the most frequently analyzed quartz variety in our laboratories.

Most natural samples were acquired as rough material from trusted dealers in the market, with a smaller number obtained directly from miners and an even smaller subset collected by the authors during unrelated field expeditions from various gravel beds. Synthetic samples were primarily purchased rough and cut directly from growers in Bangkok, though additional samples were sourced online and from the market (Jewelry Trade Center, Bangkok) to represent a broad spectrum of current synthesis conditions.

Non-polarized Fourier Transform Infrared (FTIR) spectra were collected at Bellerophon Gemlab using a Frontier Perkin Elmer FTIR spectrometer equipped with a 4x beam condenser accessory and/or a diffuse reflectance (DRIFT) module.

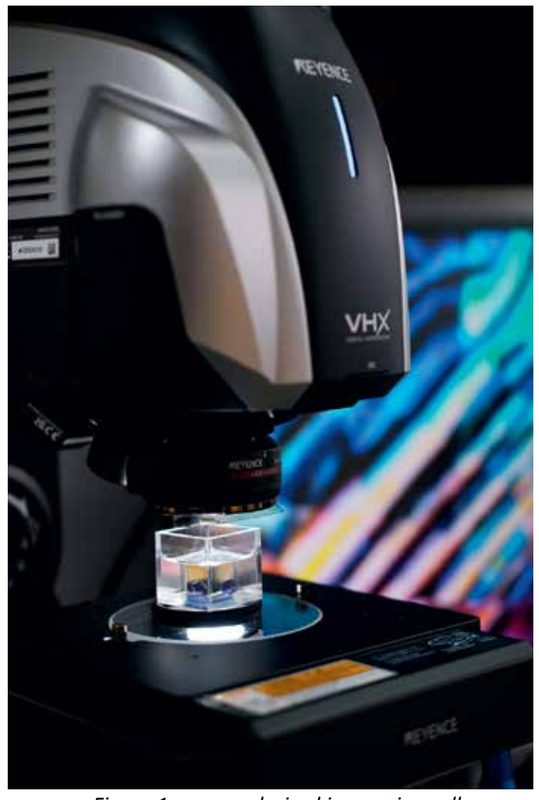

Figure 1: cross-polarized immersion cell.

QUARTZ SAMPLE TRACEABILITY GRADING

	Sample	Grades			
	n	AAA	A	B	C
Natural Quartz	50	8	9	5	28
Synthetic Quartz	50	-	-	-	50
Natural Amethyst	500	-	49	132	319
Synthetic Amethyst	500	-	-	400	100
Natural Citrine	50	-	-	-	50
Synthetic Citrine	50	-	-	40	10
Natural Smoky Quartz	50	2	22	-	26
Synthetic Smoky Quartz	50	-	-	-	50
Total	1300	10	80	577	633

AAA: Extracted the gem from the ground / Grew the gem ourselves.
A: Got the gem at the mine from the miner / Got the gem at the factory from the grower
B: Got the gem from the miner not at the mine / Got the gem from the grower not at the factory.
C: Got the gem from trusted contact in the market.

Table 1: Traceability of samples used in this study.

The spectral resolution was set to 4 cm^{-1}. Infrared spectra were recorded from multiple areas and crystallographic axes of each sample to ensure comprehensive analysis.

Micro-photography of internal inclusions was performed at Bellerophon Gemlab using a Keyence VHX-7000 system and a crossed-polarized monocular microscope fitted with a Sony 4K CMOS camera. Images were captured under various magnifications and illumination types, including a fiber optic light source. Most photographs were taken with samples immersed in an optical glass container filled with baby oil to enhance clarity (Figure 1).

For sample photography, a Canon EOS 2000D camera with a Sigma Macro DG 105-mm lens was used to ensure consistent results. Photographs were taken under standardized lighting conditions, with samples placed in a Bellerophon Gem Light Booth equipped with a 5000 K lamp.

Energy Dispersive X-ray Fluorescence (EDXRF) analysis was conducted using a Skyray EDX3000 spectrometer. Each sample underwent two analyses, with a testing time of 100 seconds per analysis, at excitation voltages of 16 kV and 45 kV.

Trace element analyses were performed at the Department of Earth Sciences "Ardito Desio," University of Milan (Italy), using an iCAP quadrupole ICP-MS coupled with a 193 nm Ar–F excimer laser. Each sample was ablated at five different spots. The laser was operated with a 65 µm spot size, 8 Hz repetition rate, and a fluence of 5 J/cm^2. Calibration was performed using the NIST612 glass standard, and internal standardization was based on 29Si utilizing a fixed stochiometric value of 99.95 wt% SiO_2. Data reduction was performed using the Glitter software suite.

Results & Discussion

Although the natural and synthetic processes for growing quartz are highly similar and comparable, subtle yet critical differences persist (Table 2).

Synthetic quartz is grown in autoclaves at temperatures and pressures broadly comparable to those of natural hydrothermal systems (Laudise, 1959). The vessels, seed racks, and cables are typically constructed from Inconel or stainless steel (Byrappa and Yoshimura, 2001) and, during the initial run of a new vessel, sodium (Na) from the mineralizer and silicate (Si) from the feed react with iron (Fe) in the chamber to form an insoluble, protective coating (Nassau, 1980).

Consequently, trace amounts of metals or ions from the autoclave, common in other hydrothermally grown gemstones (Schmetzer and Peretti, 1999), are unlikely to contaminate synthetic quartz. This pre-cludes the use of Na-containing mineralizers, such as sodium hydroxide (NaOH), in synthetic quartz intended to bear iron-related color, including the purple variety amethyst

Quartz (α-SiO_2)

	Natural Most common		Synthetic Most common		All Most common		
Variety	Mineralizer	Growth	Mineralizer	Growth	Color	Treatments	Fluid
Amethyst	NaCl	c-axis ([0001])	K_2CO_3	Z-cut (⊥ [0001]	$h^{\bullet}$-Fe^{3+}	Irradiation	H_2O
Citrine	NaCl	c-axis ([0001])	K_2CO_3	Z-cut (⊥ [0001]	Fe^{3+}	Heat (O_2)	H_2O
Crystal	NaCl	c-axis ([0001])	Na_2CO_3	Z-cut (⊥ [0001]	-	Heat (O_2)	H_2O
Smoky	NaCl	c-axis ([0001])	$NaAlO_2$	Z-cut (⊥ [0001]	$h^{\bullet}$-Al^{3+}	Irradiation	H_2O

Applied to single crystal Quartz only. Chalcedony, poly-cristalline α-SiO2 and Moganite are not included in this study. Volcanic Quartz not included in this study

Table 2: Main underlying differences between commercially available Quartz.

(colored by $h^{\bullet}$-Fe^{3+}) and the yellow variety citrine (colored by Fe^{3+} substitution), the latter artificially irradiated to produce amethyst (Cohen, 1985).

Instead, crystal growers employ most commonly potassium carbonate (K_2CO_3) as a mineralizer for iron-colored synthetic quartz, diverging from the NaOH standard used for colorless industrial crystals (Flörke et al., 1981; Balitsky et al., 2004).

In contrast, natural quartz growth relies on chloride-rich fluids (e.g., NaCl) in water as the most relevant common natural mineralizer (Fournier, 1985). Thus, synthetic quartz grown with Na-containing mineralizers should exhibit minimal iron (Fe) traces, unlike their natural counterparts.

The feed used for the growth of synthetic quartz often consists of natural quartz of lower quality and smaller size, optionally doped with ions to achieve desired colors (Byrappa and Yoshimura, 2001). Consequently, trace element analyses of synthetic quartz might be expected to closely resemble those of their natural feed counterparts.

However, our present study reveals significant differences, consistent with indirect evidence from prior work (Cohen, 1960; Karempelas et al., 2011; Balitsky et. al., 2004). Notably, these differences may manifest in the OH-related absorption bands in the infrared region (Kats, 1962; Karempelas et al., 2011), as highlighted by a non-exhaustive list of relevant spectral features in Table 3.

The divergences could stem from the mineralizer directly, such as in the uses of ammonium fluoride (NH_4F) to grow amethysts with their respective infrared absorption bands (Table 3) strongly indicative of a synthetic genesis (Balitsky et al., 2004), the use of quartz powder feeds, differences in pressure and temperature conditions, and, most critically, the differences in crystal orientation between natural and synthetic quartz (Lipson and Lang, 1975).

In synthetic quartz, seed orientation governs point defect formation (Lipson and Lang, 1975). Z-cut seeds ($\perp$ [0001]) drive rapid c-axis growth, up to 100 times faster than in natural systems (Laudise, 1959), promoting specific point defects—such as Al^{3+}-H^+ pairs and OH^- incorporation—along helical channels, which are critical for piezoelectric applications (Kats, 1962).

In contrast, R-cut seeds ({10$\bar{1}$1}) favor slower, lateral growth, increasing dislocations and altering impurity uptake (e.g., Fe^{3+}), reflecting distinct atomic exposure (Weil, 1984). Natural quartz, lacking seed control, grows along [0001] when conditions permit, but its defects reflect a variable growth environment, yielding a broader defect spectrum, including point defects and optical defects such as the famous Brazil twinning (Fournier, 1985; Crowningshield et al., 1986).

Name	Defect	Kröger-Vink Complex	Absorption (RT) nm	Absorption (RT) cm^{-1}	Emission (RT) nm	Reference
Quartz	SiO_2	$(Si_{Si}^{x}:2O_{O}^{x})^{x}$	-	340; 350; 373; 380; 415; 432; 454; 474; 663; 761; 772; 750; 1038; 1055;1138; 1201	-	Winta et al, 2018 Oranges, *n.a*
	Li^{+}-OH	$(OH_{O}^{\bullet}:Li_{Si}^{'''})^{''}$	-	3483	-	Baron et al, 2015 Jollands et al, 2020
	Fe^{3+}	$Fe_{Si}^{'}$	Broad ~400; 450	-	-	Nassau, 1980
Al color center	$h^{\bullet}$-Al^{3+}	$(O_{O}^{\bullet}:Al_{Si}^{'})^{x}$	Broad ~200 to 800 375; 475; 730	-	-	Nassau, 1980
Fe color center	$h^{\bullet}$-Fe^{3+}	$(O_{O}^{\bullet}:Fe_{Si}^{'})^{x}$	300; 348; 545	-	-	Nassau, 1980
	Al^{3+}-OH	$(OH_{O}^{\bullet}:Al_{Si}^{'})^{x}$	-	3313; 3379; 3430	-	Kats, 1962 Jollands et al, 2020
	B^{3+}-OH	$(OH_{O}^{\bullet}:B_{Si}^{'})^{x}$	-	3595	-	Staats & Kopp, 1985 Jollands et al, 2020
	Si_2OH^{-}	$(OH_{O}^{\bullet}:Si_{Si}^{x})^{\bullet}$	-	3585	-	Lipson & Kahan, 1985 Jolland et al, 2020
3543	$_z[FeO4]^{\bullet}$-OH	-	-	3543	-	Balitsky et al, 2004
	NH_4F- related	-	-	3630; 3664; 3680	-	Balitsky et al, 2005
O hole center	NBOHC	-	-	-	600	Ricci et al, 2021

Many of these complex, expressed in Kroger-Vink notation, might be understood and/or speculated, while others might be recognized based on their associated defect.

Table 3: Relevant non-exhaustive spectral defects in Quartz.

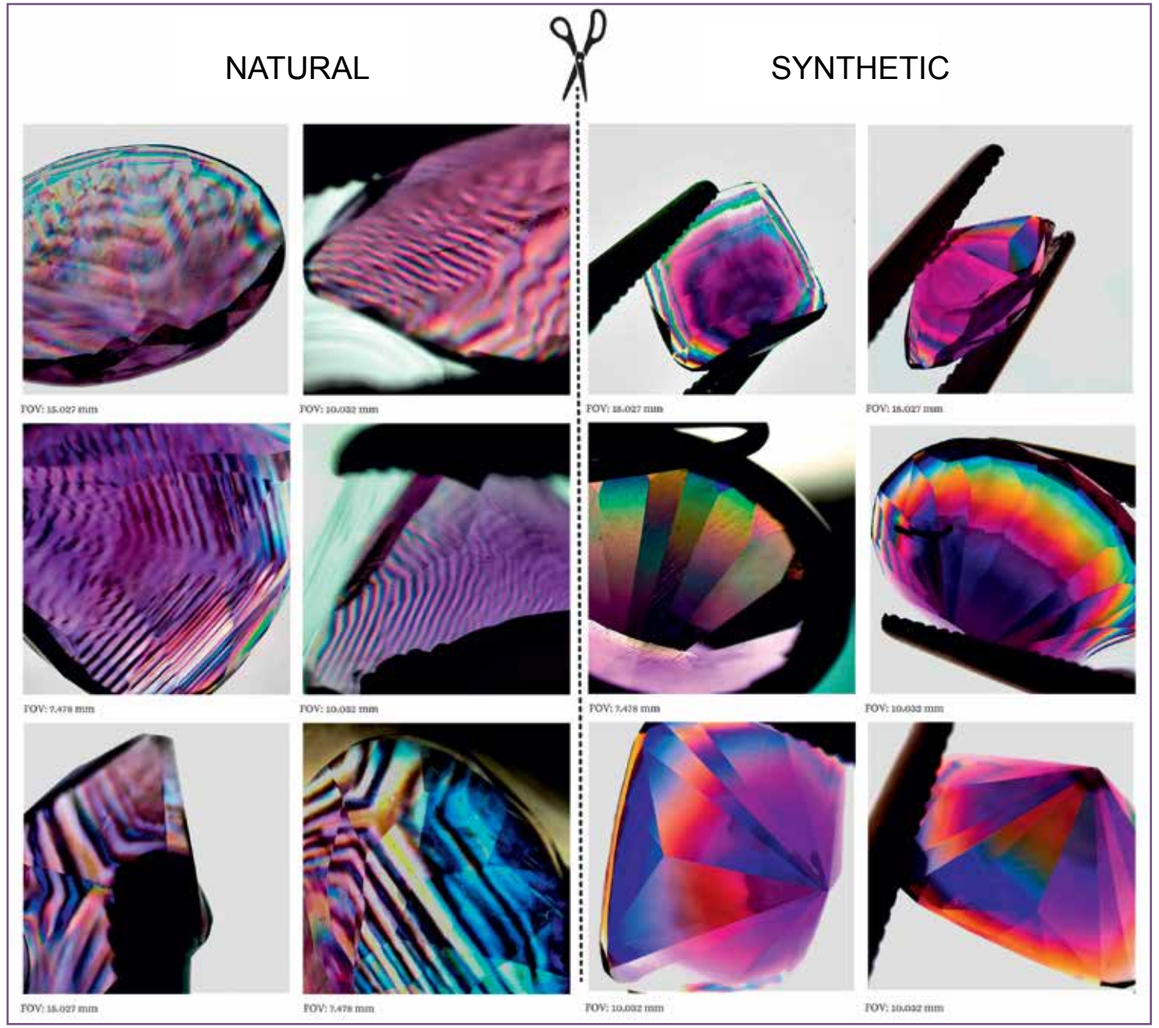

Figure 2: Natural and synthetic Amethyst interference patterns under cross-polarized light.

Amethyst

From the thousand amethyst samples tested, a remarkable pattern emerges. Brazil twinning manifests as lamellar or sector patterns in quartz, visible under crossed polarizers as interference colors or extinction bands (Figure 2). It arises from stress, temperature fluctuations, or chemical gradients during natural hydrothermal growth, destabilizing the lattice and promoting twin boundary formation. In contrast, synthetic amethyst, grown under controlled conditions, rarely exhibits Brazil twinning due to crystal orientation, uniform temperature, pressure, and fluid chemistry that minimize such disruptions, manifesting instead as regular interference colors in a flame-like pattern (Figure 2). This distinction positions Brazil twinning as a key diagnostic feature for differentiating natural from synthetic amethyst, first noted by Crowningshield in 1986. However, although none was observed in our study, synthetic quartz and synthetic amethyst with Brazilian twinning are known to exist, typically resulting from the use of natural twinned quartz as seeds (Koivula and Fritsch, 1989; Schmetzer, 1989; Sunagawa et al., 1990). Therefore, relying solely on Brazil twinning may prove potentially misleading.

The 3595 cm^{-1} band, widely recognized today as a hallmark of natural amethyst (Karampelas et al., 2011), is associated with OH defects linked to boron substitution (B^{3+}-OH) (Jollands et al., 2020). It is present in 97% of our natural samples but absent in all synthetic ones (Figure 3), validating its potential as a diagnostic tool for distinguishing natural from synthetic amethyst.

However, this 3595 cm^{-1} absorption band is known to occur in synthetic quartz doped with boron (Staats and Kopp, 1974; Brown and Kahan, 1975; Thomas et al., 2009; Baron et al., 2015; Jollands et al., 2020). Relying solely on its presence to identify natural amethysts is highly risky, since its absence does not definitively confirm an amethyst as synthetic.

The 3543 cm^{-1} band is surprisingly present in all synthetic amethyst samples and absent in all our natural samples (Figure 3). This feature, widely studied and attributed to OH defects possibly linked to alkali- or Fe-related defects, is considered specific to amethyst.

Although absent in our natural samples, it has been documented in many natural amethyst samples from specific deposits (Balitsky et al., 2004; Karampelas et al., 2005; Karampelas et al., 2011). Consequently, as with the previous criteria, this feature alone must be interpreted with great caution.

Trace elements offer critical insights into the genesis of amethysts. All our natural samples exhibit gallium, averaging ~3 ppm, while synthetic samples show no gallium above our instrument's detection limit (<0.5 ppm), consistent with previous research (Balitsky et al., 1999; Müller et al., 2003; Götze et al., 2005; Götze, 2009; Lameiras et al., 2010).

Aluminum, the most abundant trace element alongside iron in all samples, is known to associate with gallium in many natural gemstones, rendering its presence unsurprising.

However, aluminum is, on average, higher in synthetic amethyst (Table 4) most likely reflecting purified feed materials adhering to industrial purity standards, eliminating most gallium and possibly boron, or the Z-cut seed orientation restricts the incorporation of related defects into the crystal lattice.

While invaluable, relying solely on gallium must be approached with caution, as synthetic quartz doped with gallium up to 15 ppm has been produced experimentally (Hosaka and Taki, 1981; Weil, 1984; Müller et al., 2003; Brown and Kahan, 1975).

Conversely, natural quartz from veins with gallium content as low as 0.01 ppm has been documented (Müller et al., 2003). Many trace elements analyzed by LA-ICP-MS do not appear to be useful for differentiating between natural and synthetic materials (Figure 4), with the notable exception of boron and niobium.

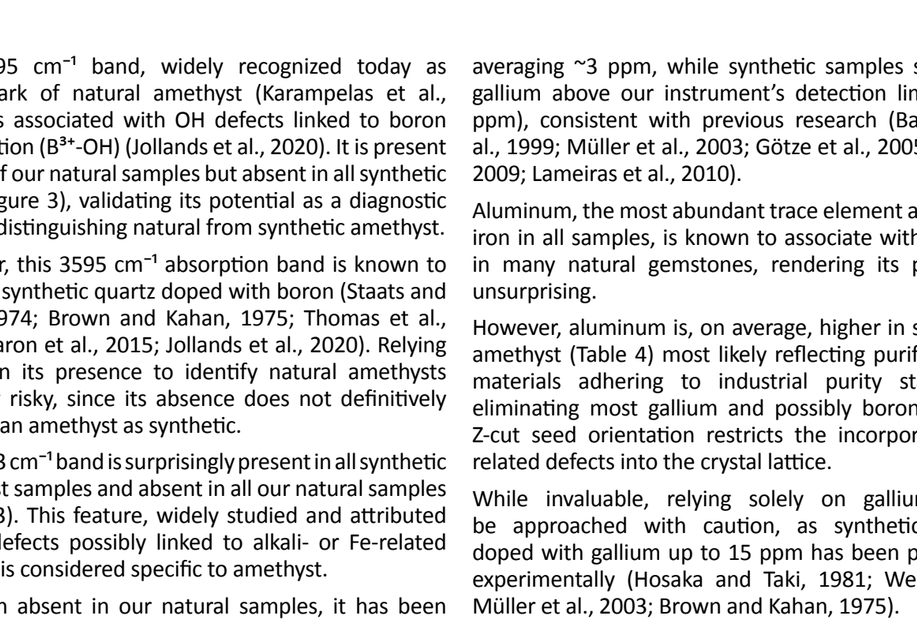

Figure 3: Relevant OH-related absorption features of Amethyst.

Figure 4: Amethyst trace elements by LA-ICP-MS. All values are reported in ppm.

NATURAL AMETHYST														
	Li	Be	B	Al	Si	P	Ti	Ge	Rb	Sr	Nb	Sn	Sb	La	Yb	Ta	W
Range	2.89-10.94	0.026-0.116	1.518–4.712	0.289–19.334	467205.684–696	38.356–42.506	5.252–8.834	0.14-0.509	0.014-0.017	0.002-0.149	0.001-0.011	0.034-0.823	0.018-0.097	0.583–21.241	0.0016-0.0083	0.0005-0.004	0.0015-0.5462
Average	6.32	0.068	2.925	6.167	467205.691	39.760	6.084	0.370	0.0153	0.052	0.0053	0.203	0.036	10.345	0.0035	0.0019	0.073
Median	5.47	0.070	2.748	2.982	467205.690	39.077	5.681	0.385	0.0155	0.035	0.0043	0.081	0.026	9.268	0.0029	0.0016	0.004

SYNTHETIC AMETHYST																	
	Li	Be	B	Al	Si	P	Ti	Ge	Rb	Sr	Nb	Sn	Sb	La	Yb	Ta	W
Range	7.49-15.64	0.02-0.301	0.38–0.788	9.044–43.366	467205.494–.732	36.832–46.858	5.908–9.004	0.049-0.799	0.012-0.075	0.003-0.039	0.001-0.003	0.037-0.189	0.029-0.084	0.001-17.785	0.0014-0.0034	0.0004-0.0063	0.0011-0.01
Average	11.33	0.055	0.529	16.409	467205.637	42.115	6.923	0.290	0.020	0.011	0.0019	0.081	0.053	3.955	0.0024	0.0018	0.003
Median	11.29	0.024	0.54	13.084	467205.660	41.724	6.800	0.254	0.014	0.007	0.0018	0.073	0.052	0.548	0.0026	0.0009	0.002

Table 4: Amethyst trace element profiles (in ppm), of 15 synthetic samples vs 9 natural samples.

AMETHYST GENESIS IDENTIFICATION			
Name	n^{500} Natural	n^{500} Synthetic	Cause
Brazilian Twinning	100%	0%	Crystal orientation
3595 cm^{-1}	97%	0%	$(OH_O^{\bullet}:B_{Si}^{/})^x$
3543 cm^{-1}	0%	100%	$_z[FeO4]^{\bullet}$-OH
Gallium >1 ppm	100%	0%	$Ga_{Si}^{/}$

n = number of sample tested.

Table 5: Combined keys feature of natural and synthetic Amethyst.

Author V. Fejoz preparing samples for liquid-nitrogen photoluminescence analysis of Amethyst. The image is not discussed in the main text because the analyses did not yield conclusive results. It highlights the significant number of unreported and inconclusive experiments that underpin each research conclusion.

Conclusion

Combining these four features (Table 5) yields an undeniable pattern for the identification and differentiation of natural and synthetic amethyst. Although each feature is theoretically possible, individually, in either natural or synthetic amethyst, the probability of all four occurring together in laboratory-grown amethyst remains, to date, highly unlikely. Lastly, the additional use of quantitative aluminum, lithium, and niobium data should help differentiate any unclear cases.

Further Discussion

This study (Part I) includes only the Amethyst variety; Citrine, Crystal Quartz, and Smoky Quartz will be included in Part II.

References

Balitsky, V. S., Lu, T., Rossman, G. R., Makhina, I. B., Mar'in, A. A., Shigley, J. E., Elen, S., and Dorogovin, B. A. (1999). "Russian Synthetic Ametrine." *Gems & Gemology,* 35(2), 122–134. DOI: 10.5741/GEMS.35.2.122.

Balitsky, V. S., Balitsky, D. V., Bondarenko, G. V., and Balitskaya, O. V. (2004). "The 3543 cm^{-1} Infrared Absorption Band in Natural and Synthetic Amethyst and Its Value in Identification." *Gems & Gemology,* 40(2), 146–161. DOI: 10.5741/GEMS.40.2.146.

Baron, M. A., Stalder, R., and Konzett, J. (2015). "OH Defects in Quartz from Granite-Related Hydrothermal Systems: An Infrared Spectroscopic Study." *European Journal of Mineralogy*, 27(4), 513–522. DOI: 10.1127/ejm/2015/0027-Brown, R. N., and Kahan, A. (1975). "Hydrothermal Synthesis, Optical Perfection, and Surface Topography of Quartz Grown in RbOH and Other Alkali Hydroxides." *Journal of Crystal Growth*, 30(1), 83–92. DOI: 10.1016/0022-0248(75)90031-0.

Byrappa, K., and Yoshimura, M. (2001). Handbook of Hydrothermal Technology. William Andrew Publishing. ISBN: 978-0815514459.

Cohen, A. J. (1960). "Substitutional and Interstitial Aluminum in Synthetic Quartz." *Journal of Physics and Chemistry of Solids*, 13(3-4), 321–325. DOI: 10.1016/0022-3697(60)90015-8.

Cohen, A. J. (1985). "Amethyst Color in Quartz, the Result of Radiation Damage and Iron Impurities." *American Mineralogist*, 70(11-12), 1180–1185.

Crowningshield, R., Hurlbut, C., and Fryer, C. W. (1986). "A Simple Procedure to Separate Natural from Synthetic Amethyst on the Basis of Twinning." *Gems & Gemology*, 22(3), 130–139. DOI: 10.5741/GEMS.22.3.130.

Flörke, O. W., et al. (1981). "Hydrothermal Synthesis of Quartz with Potassium Carbonate as Mineralizer." *Crystal Research and Technology*, 16(5), 587–592. DOI: 10.1002/crat.19810160512.

Fournier, R. O. (1985). "The Behavior of Silica in Hydrothermal Solutions." *Reviews in Economic Geology*, 2, 45–61.

Fritsch, E., and Rossman, G. R. (1987). "An Update on Color in Gems. Part 1: Introduction and Colors Caused by Dispersed Metal Ions." *Gems & Gemology,* 23(3), 126–139. DOI: 10.5741/GEMS.23.3.126.

Götze, J., Plötze, M., and Trautmann, T. (2005). "Structure and Luminescence Characteristics of Quartz from Pegmatites." *American Mineralogist,* 90(1), 13–21. DOI: 10.2138/am.2005.1561.

Götze, J. (2009). "Chemistry, Textures and Physical Properties of Quartz – Geological Interpretation and Technical Application." *Mineralogical Magazine,* 73(4), 645–671. DOI: 10.1180/minmag.2009.073.4.645.

Hosaka, M., and Taki, S. (1981). "Growth Mechanism of Quartz Crystals Doped with Trivalent Metal Ions." *Journal of Crystal Growth,* 52(1), 837–842. DOI: 10.1016/0022-0248(81)90202-8.

Jollands, Michael C., Marc Blanchard, Etienne Balan. Structure and theoretical infrared spectra of OH defects in quartz. *European Journal of Mineralogy,* Copernicus, 2020, 32 (3), pp.311-323. ff10.5194/ejm-32-311-2020ff.

Karampelas, S., Fritsch, E., Zorba, T., and Paraskevopoulos, K. M. (2011). "Infrared Spectroscopy of Natural vs. Synthetic Amethyst: An Update." *Gems & Gemology,* 47(3), 196–201. DOI: 10.5741/GEMS.47.3.196.

Karampelas, S., Fritsch, E., Zorba, T., Paraskevopoulos, K. M., and Sklavounos, S. (2005). "The 3543 cm^{-1} Infrared Absorption Band in Natural and Synthetic Amethyst and Its Value in Identification." *Gems & Gemology,* 41(4), 334–341. DOI: 10.5741/GEMS.41.4.334.

Kats, A. (1962). "Hydrogen in Alpha-Quartz." *Philips Research Reports,* 17, 133–195.

Koivula, J. I., and Fritsch, E. (1989). "The Growth of Brazil-Twinned Synthetic Quartz and the Potential for Synthetic Amethyst Twinned on the Brazil Law." *Gems & Gemology,* 25(3), 159–164. DOI: 10.5741/GEMS.25.3.159.

Lameiras, F. S., Nunes, E. H. M., and Vasconcelos, W. L. (2010). "Spectroscopic Study of Natural Quartz Samples." Radiation Effects and Defects in Solids, 165(1), 66–74. DOI: 10.1080/10420150903373254.

Laudise, R. A. (1959). "Kinetics of Hydrothermal Quartz Crystallization." *Journal of the American Chemical Society*, 81(3), 562–566. DOI: 10.1021/ja01512a015.

Lipson, H., and Lang, A. R. (1975). "Defects in Quartz and Their Relation to Crystal Growth." *Journal of Crystal Growth*, 28(3), 365–370. DOI: 10.1016/0022-0248(75)90107-8.

Müller, A., Wiedenbeck, M., Van den Kerkhof, A. M., Kronz, A., and Simon, K. (2003). "Trace Elements in Quartz – A Combined Electron Microprobe, Secondary Ion Mass Spectrometry, and Cathodoluminescence Study." *European Journal of Mineralogy,* 15(4), 747–763. DOI: 10.1127/0935-1221/2003/0015-0747.

Nassau, K. (1980). Gems Made by Man. Chilton Book Company. ISBN: 978-0801967733.

Schmetzer, K., and Peretti, A. (1999). "Some Diagnostic Features of Russian Hydrothermal Synthetic Rubies and Sapphires." *Gems & Gemology,* 35(1), 17–28. DOI: 10.5741/GEMS.35.1.17.

Schmetzer, K. (1989). "Types of Twinning in Natural and Synthetic Amethyst." *Journal of Gemmology,* 21(6), 356–365. DOI: 10.15506/JoG.1989.21.6.356.

Staats, P. A., and Kopp, J. (1974). "Detection of OH Absorption Bands in Boron-Doped Synthetic Quartz." *Journal of Crystal Growth*, 22(1), 65–68. DOI: 10.1016/0022-0248(74)90097-2.

Sunagawa, I., Taijing, L., and Balitsky, V. S. (1990). "Generation of Brazil and Dauphiné Twins in Synthetic Amethysts." *Physics and Chemistry of Minerals*, 17(4), 320–325. DOI: 10.1007/BF00200127.

Thomas, S. M., Koch-Müller, M., Reichart, P., Rhede, D., Thomas, R., and Wirth, R. (2009). "IR Calibrations for Water Determination in Olivine, Geikielite, and Quartz." *Physics and Chemistry of Minerals,* 36(8), 489–509. DOI: 10.1007/s00269-009-0292-8.

Weil, J. A. (1984). "A Review of Electron Spin Resonance in Quartz: The State of the Art." *Journal of Applied Physics,* 55(6), 1429–1440. DOI: 10.1063/1.333479.

Weil, J. A. (1984). "A Review of Electron Spin Resonance in Quartz: The State of the Art." *Journal of Applied Physics,* 55(6), 1429–1440. DOI: 10.1063/1.333479.

All images are courtesy of Bellerophon. ◊